(Preprint) AAS 20-741

SOLAR SYSTEM ESCAPE TRAJECTORIES USING OUTER PLANETARY GRAVITY ASSISTS

Rohan Patel[*], Damon Landau[†], and Try Lam[‡]

A broad search of outer planet gravity assist sequences reveals flyby conditions that are naturally amenable for solar system escape. The optimal flyby conditions depend on the arrival velocity at the final body and provide the maximum possible escape speed for purely ballistic sequences. Trajectories in the 2030-2060 time frame are categorized by their encounter year with an emphasis on solar system escape speed and direction. All resulting sequences require a Jupiter gravity assist, and a considerable increase in escape speed is found in trajectories that utilize an additional Saturn, Uranus, or Neptune flyby. However, these solutions are limited by their availability and range of right ascensions. All cataloged trajectories are able to escape the solar system at least 3 au/year, and the highest energy sequences are in excess of 5.5 au/year. The search space is then used to find outer planet gravity assist trajectories to Kuiper Belt Objects (KBOs), and several cases are optimized.

INTRODUCTION

Missions to study the outer solar system, fly-by Kuiper Belt Objects (KBOs), or conduct interstellar science commonly rely on solar system escape trajectories with reasonable mission durations. Ballistic gravity assists of the outer planets is a method that has been employed by all previous missions to attain the required escape energy. Legacy spacecraft like Pioneer 10 and 11 were among the first man made objects launched on these trajectories, and the Voyager mission followed with the exploration of the outer planets and an escape into interstellar space. A recent mission to the near-interstellar medium is New Horizons, and it is currently leaving the solar system following a Jupiter gravity assist and Pluto flyby. The escape speeds of the active spacecraft are listed in Table 1. Apart from conventional trajectory design techniques, novel solar system escape methods include the use of solar sails[1,2] and a perihelion or Jovian powered flyby.[1]

A broad trajectory search is often the first step in interplanetary mission design[3] as it helps to map out the solution space and catalog feasible flyby combinations with their encounter characteristics. A common search method is to use the zero sphere of influence assumption and Lambert arcs to create trajectories using the patched conics model.[4] While this method doesn't optimize solutions, it is a useful starting point for the design process. Broad searches have been conducted to find trajectories to the outer planets. Spreen et al.[5] investigated ballistic gravity assist trajectories to Uranus from 2020-2060. Hughes et al.[6] conducted a similar search to map out possible trajectories

[*]Undergraduate Student, Aerospace Engineering, Cal Poly Pomona, 3801 W Temple Ave., Pomona, California, 91786
[†]Mission Formulation Engineer, Systems Engineering Section, Jet Propulsion Laboratory, California Institute of Technology, 4800 Oak Grove Dr., Pasadena, CA, 91109
[‡]Mission Design Engineer, Mission Design and Navigation Section, Jet Propulsion Laboratory, California Institute of Technology, 4800 Oak Grove Dr., Pasadena, CA, 91109

Table 1: Active spacecraft on escape trajectories.

Spacecraft	Escape Speed in au/year
Voyager 1	3.58*
Voyager 2	3.24*
New Horizons	3.05[10]

to Neptune using Jupiter or Saturn flybys in the years 2020-2070. A Jupiter gravity assist was found to be beneficial in reducing the required launch energy and time-of-flight (TOF). Direct transfers to Saturn were also used for when Jupiter transfers were not available, but these required higher launch energies. KBO trajectory searches suggest that a Jupiter flyby and a combination of outer planet flybys can significantly reduce the flight time, and common sequences to certain KBOs were also noticed.[7–9] Trajectories to Makemake arriving in 2054 exist with a Jupiter-Saturn flyby and another opportunity in 2035 uses a Jupiter gravity assist. Similarly, Haumea encounters in 2035, 2043, and 2044 and Quaoar encounters in 2036 and 2046 all were found to have a Jupiter flyby.

In this paper, we first conduct a broad search to find possible outer planet gravity assist trajectories between the years 2030 and 2060. Optimal flyby conditions that maximize the energy with respect to the sun are applied to each trajectory, and their resulting outgoing speed and direction are cataloged. We extend the outer planet flyby search to find trajectories to KBOs with absolute magnitudes less than or equal to 4 from the Jet Propulsion Laboratory's Small-Body Database†. Several KBO trajectories are optimized and cataloged.

TRAJECTORY SEARCH, FLYBY, AND PROPAGATION

Trajectory Search

The search algorithm uses the patched conics model to build gravity-assist sequences. The total number of encounters in the trajectory is set a priori with a pool of candidate flyby bodies specified for each encounter. In our case we ran two searches: 1) two encounters with an Earth departure followed by a flyby of either Jupiter or Saturn, and 2) three encounters that depart Earth, flyby Jupiter or Saturn, then flyby Saturn, Uranus, or Neptune. Later, we extend this to include a KBO as a third or fourth encounter in the sequence. The search is performed by computing Lambert fits for all possible transfers for each leg, where the encounter times are derived from user-defined time steps, bounds on encounter dates, and bounds on relative flight times, as indicated in Table 2. The dimension of the search space remains manageable because the position at the conic endpoints are derived from the body ephemerides, enabling a two-dimensional search for each leg.[11,12] The Lambert-fit and body velocities provide a set of arrival and departure relative velocity (V_∞) vectors for each encounter, and all possible gravity assists are then computed. Because the arrival and departure V_∞ are computed independently, a small ΔV is required to patch each flyby. In our case we limit the flyby ΔV (beyond what is naturally provided by the gravity assist) to less than 10 m/s, producing ballistic sequences with refinement in an optimizer following the broad search. Trajectories that maximize the incoming relative velocity (V_∞^-) have the potential to maximize the energy gained through the flyby. The design parameters for the search are summarized in Table 2.

Figure 1 shows the resulting trajectories sorted by their final encounter body (left plot) and the required Earth departure characteristic energy (C_3) (right plot). Solutions that escaped the solar

*https://voyager.jpl.nasa.gov/mission/status/

†https://ssd.jpl.nasa.gov/

Table 2: Search Input Criteria

Parameter	Value
Earliest Launch Year	2030
Final Body Encounter Year	2031-2060
Earth Departure C_3	$\leq$121 km^2/s^2
Number of Gravity Assists	1 or 2 (separate runs)
Flyby Bodies	Jupiter, Saturn, Uranus, Neptune
Minimum Flyby Altitude	5,000 km (80,000 km for Saturn)
Epoch Time Steps	3 days
Max. Impulsive ΔV at flyby	10 m/s
Max. Interplanetary Flight Time	3000 days
Minimum Escape Speed	3 au/year

system at less than 3 au/year were discarded. This constraint removed all direct Saturn transfers despite accommodating for them with a relatively high launch C_3. The resulting data was filtered further by the final encounter body with an additional flight time limit to remove long duration sequences to Saturn or Uranus with low incoming relative velocity magnitudes. As a result, Jupiter-Saturn gravity assists (JSGA) with flight times greater than 5.5 years and Jupiter-Uranus (JUGA) solutions of past 7 years were removed. The Jupiter only gravity assists (JGA) solutions make up a large sum of the search results. Jupiter-Uranus and Jupiter-Neptune (JNGA) gravity assists offer high a V_∞^-, but at the expense of significantly longer time spent interplanetary. Nearly all high V_∞ solutions maximized the launch energy.

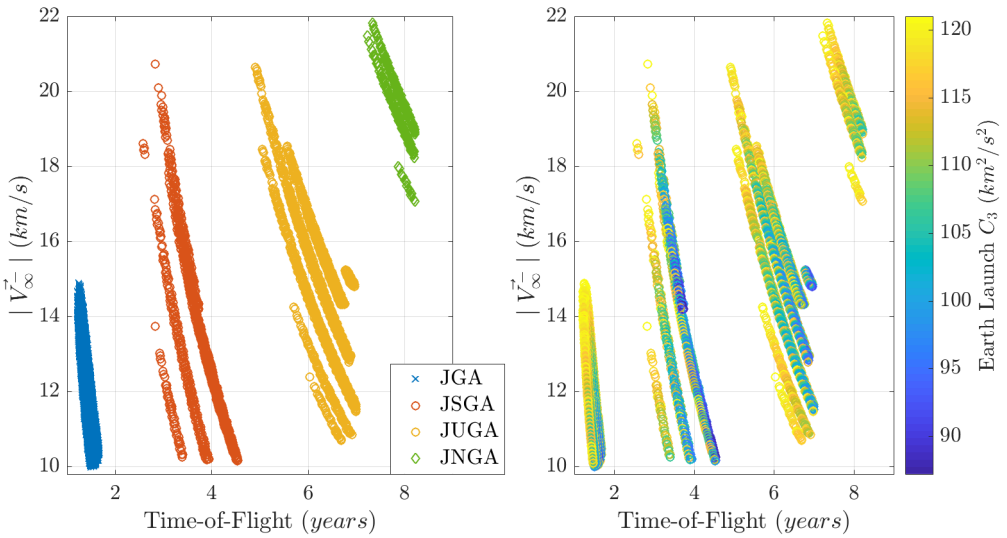

Figure 1: Broad search trajectories sorted by time of flight in years, V_∞ (km/s), and Earth departure energy (C_3). Neptune trajectories are limited by the TOF constraint, and JSGAs are limited by the upper date limit set for the search space.

Energy Maximizing Flyby Conditions

With the intent to ballistically escape the solar system, the final flyby should maximize the heliocentric energy of the trajectory. To do this, we start with the vis-viva energy equation:

$$2\varepsilon = C_3 = (\mid \vec{V_p} + \vec{V_\infty^+} \mid)^2 - \frac{2\mu}{r} \tag{1}$$

where μ is the standard gravitational parameter and r is the radial distance. The heliocentric velocity vector is the summation of the flyby body's velocity around the Sun ($\vec{V_p}$) and the trajectory's relative velocity vector with respect to the flyby body at the asymptote ($\vec{V_\infty^+}$). The superscript in the relative velocity term is negative for the incoming or positive for the outgoing vectors. By inspection, the energy of the trajectory is maximized when the velocity and radial distance is maximized. The following relation for the heliocentric velocity can be made:

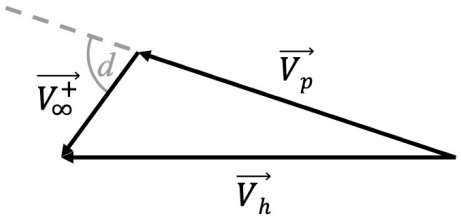

Figure 2: Post-flyby velocity triangle where $\vec{V_h}$ is the heliocentric velocity of the spacecraft, $\vec{V_p}$ is the planet's heliocentric velocity, and $\vec{V_\infty^+}$ is the outgoing relative velocity at the asymptote.

$$V_h^2 = V_p^2 + V_\infty^{+2} + 2V_pV_\infty^+ cos(d) \tag{2}$$

It is seen that as angle d between $\vec{V_p}$ and $\vec{V_\infty^+}$ approaches 0, the magnitude of the heliocentric velocity is maximized. This condition can be restated as:

$$C = \cos(d) = \hat{V_p} \cdot \hat{V_\infty^+} \tag{3}$$

The heliocentric velocity of the body at the flyby epoch and the trajectory's incoming relative velocity vector are known from the search. The outgoing $\vec{V_\infty^+}$ can be parametrized by the bending (δ) and crank (τ) angles in the B-Plane coordinate frame as defined in Figure 10 of the Appendix.

$$\vec{V_\infty^+} = V_\infty[\cos(\delta)\hat{S} - \sin(\delta)\cos(\tau)\hat{T} - \sin(\delta)\sin(\tau)\hat{R}] \tag{4}$$

Eq. (2) and $\hat{V_p}$ in the B-Plane frame (see Appendix) can be substituted into Eq. (3) as:

$$C = V_{p_s}\cos(\delta) - V_{p_t}\sin(\delta)\cos(\tau) - V_{p_r}\sin(\delta)\sin(\tau) \tag{5}$$

The optimal crank angle can be found by setting the partial of C with respect to τ equal to 0.

$$\frac{\partial C}{\partial \tau} = V_{p_t}\sin(\delta)\sin(\tau) - V_{p_r}\sin(\delta)\cos(\tau) \tag{6}$$

After rearranging terms the following expression for the optimal crank angle (B-Plane angle) is found:

$$\tau_{opt.} = \tan^{-1}(\frac{V_{p_r}}{V_{p_t}}) \tag{7}$$

The following relations are derived from Eq. (7) and Eq. (5) to maximize C which can then be used to find δ_{opt}:

$$\sin(\tau_{opt.}) = \frac{-V_{p_r}}{\sqrt{V_{p_r}^2 + V_{p_t}^2}} \tag{8}$$

$$\cos(\tau_{opt.}) = \frac{-V_{p_t}}{\sqrt{V_{p_r}^2 + V_{p_t}^2}} \tag{9}$$

The optimal bending angle can now be solved by taking the partial of C with respect to δ and substituting in the result from Eq. (7). The partial is found as:

$$\frac{\partial C}{\partial \delta} = -V_{p_s}\sin(\delta) - V_{p_t}\cos(\delta)\cos(\tau_{opt}) - V_{p_r}\cos(\delta)\sin(\tau_{opt}) \tag{10}$$

and is set to 0 to find the extremal. With the relations from Eq. (8) and Eq. (9), Eq. (10) is simplified to:

$$V_{p_s}\sin(\delta) = \cos(\delta)\sqrt{V_{p_r}^2 + V_{p_t}^2} \tag{11}$$

$$\delta_{opt.} = \tan^{-1}\left(\frac{\sqrt{V_{p_r}^2 + V_{p_t}^2}}{V_{p_s}}\right) \tag{12}$$

Recall that the $\hat{V_p}$ is a unit vector. The relationship for the optimal flyby bending angle is now found as:

$$\delta_{opt.} = cos^{-1}(V_{p_s}) \tag{13}$$

and its associated flyby altitude is defined as:

$$r_{alt} = \frac{\mu}{\mid V_\infty^2 \mid}\left(\frac{1}{sin(\frac{\delta_{opt}}{2})} - 1\right) - r_{body} \tag{14}$$

For cases where the close approach altitude computed from the optimal bending angle is lower than the constraint, Eq. (14) can be rearranged to find the associated δ at the r_{min} radius as:

$$\delta = 2\sin^{-1}\left(\frac{1}{1 + \frac{r_{min}V_\infty^2}{\mu}}\right) \tag{15}$$

Now the bending and crank angles can be substituted into Eq. (4), and the planet's velocity vector is added to find the heliocentric velocity post-flyby. For this paper, the characteristic energy (C_3) is also referenced to categorize trajectories as found from Eq. (1).

Post-Flyby Propagation

The state vector of the trajectory can now be formed using the post-flyby heliocentric velocity and the assumption that the position of the trajectory is approximately the body's position at the flyby epoch. It can be represented in Keplerian elements, and the time since periapsis is found using the hyperbolic eccentric anomaly (H). For some change in time (dt), the new state can be found using Kepler's equation of a hyperbola.

$$M = e\sinh(H) - H \tag{16}$$

The new mean anomaly is found by iterating on Kepler's equation, and conics are propagated forward to determine its post-flyby path. Once the propagated true anomaly is found, the state is converted back to cartesian coordinates in the perifocal frame. A frame transformation is done to represent the state vector in the Mean Ecliptic J2000 frame.

ESCAPE TRAJECTORIES AND SEARCH SPACE

Energy Maximizing Flyby Characteristics

Across the search space, certain flyby characteristics are seen to maximize the solar system escape speed. Figure 3 shows the proportional relationship between the post flyby energy and incoming relative velocity for the sequence types. The incoming relative velocity magnitude has a significant contribution to the energy. Sequence types that have multiple sets of encounter years exhibit variations that suggest the V_∞ direction (relative to V_p) also influences the energy gain.

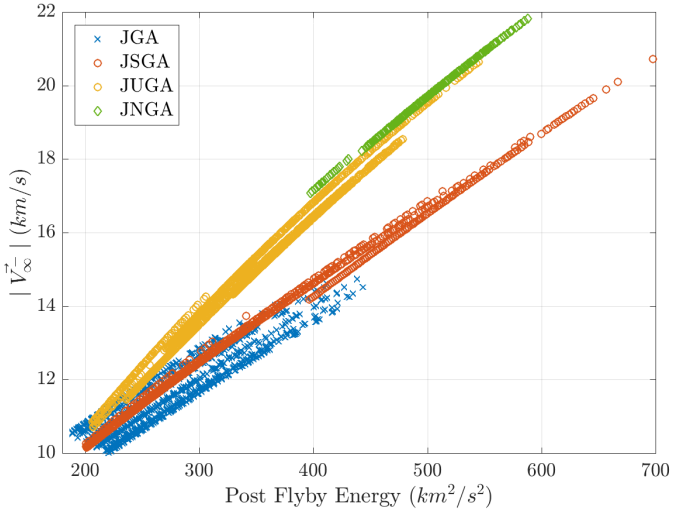

Figure 3: Final flyby incoming relative velocity versus outgoing C_3. Relative to each body, as the magnitude of V_∞ increases the post flyby energy also increases.

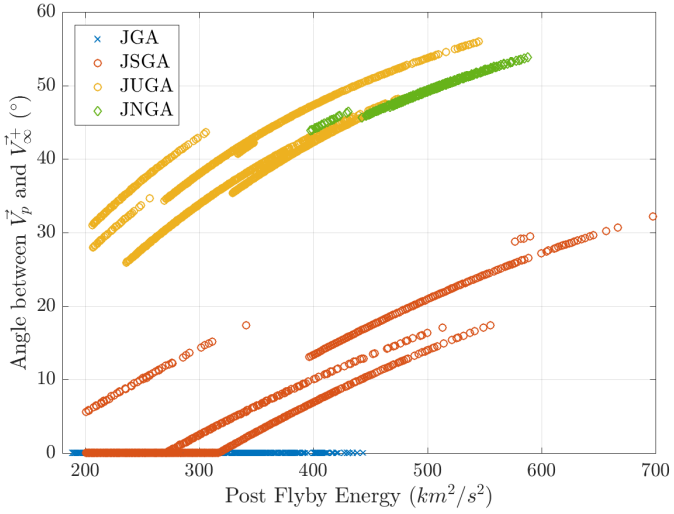

Figure 4: Angle between $\vec{V_p}$ and $\vec{V_\infty^+}$ versus energy. The altitude constraint limits the bending angle and in return the angle between the two velocities.

Figure 4 shows the angle *d*, from Figure 2, between the planet's velocity and the outgoing relative velocity vectors. The results appear contrary to the expected condition from Eq. (3), but this is only because most of the searched conditions reach the minimum flyby altitude. The constraint makes

the bending angle solely a function of the incoming relative velocity magnitude, which is seen in Figure 3. This means, that as the $\vec{V_\infty}$ increases, the difference between the optimal bending angle and the bending capability of the body increases, hence the increase in d in Figure 4. All Jupiter trajectories in the search results are fully optimal because angle d is 0 degrees in all cases. Saturn is able to sufficiently bend the trajectory in cases where the incoming V_∞ is low enough, but then becomes limited by the large flyby altitude constraint. All flybys of Uranus and Neptune reached the minimum flyby altitude.

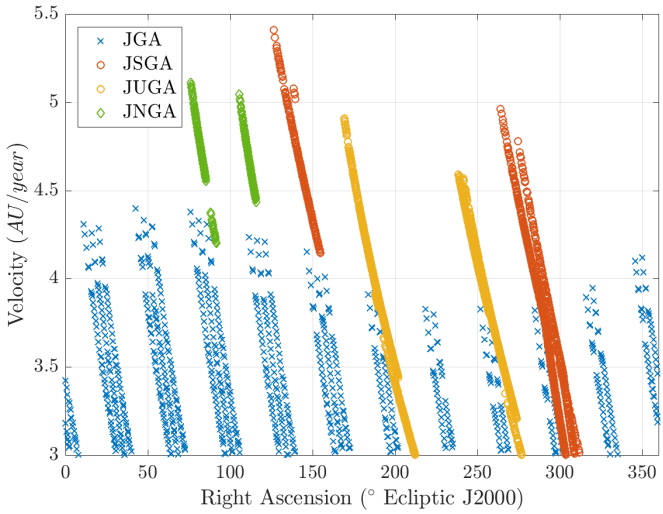

Figure 5: Escape speed (au/year) versus direction ($°RA$)

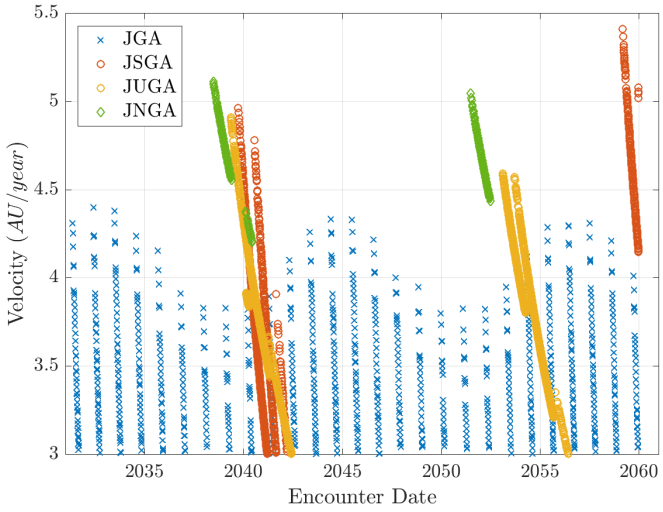

Figure 6: Search space summary of the escape speed (au/year)

Figure 5 and Figure 6 categorize right ascensions and encounter date with the escape velocity at the asymptote. The JGA sequence is able to cover a broad range of escape directions, but at the expense of speed. Due to the multi-body nature of rest of the sequences, these trajectories can be quicker, but are significantly limited in their directions. The broad search results are categorized below by their sequence type, availability, escape direction, and speed. The escape direction is represented by the outgoing asymptote's right ascension in the Mean Ecliptic J2000 frame.

Search Space by Trajectory Type

Jupiter Only Gravity Assist JGA trajectories provide regular launch opportunities approximately every 13 months due to the synodic period between Earth and Jupiter (when compared to multi-flyby trajectories). The highest energy years are 2032, 2044, and 2056 as seen in Figure 6, and the gap between these years coincide with the nearly 12 year orbital period of Jupiter indicating that its heliocentric state is correlated with the maximize escape energy. The Earth-Jupiter transfer durations are around 450 days and the incoming relative velocity is roughly 14.7 km/s. Top performing trajectories all have flyby altitudes around 43,000 km with a subsequent bending angle of 113 degrees. The large bending capability of Jupiter ensures that the maximum attainable post-flyby heliocentric velocity is not constrained by the minimum flyby altitude. Table 3 contains the range of solutions grouped by the earliest and latest Jupiter encounter dates and their associated Earth launch dates. The exact start and stop dates of the encounters are presented in this table instead of by a yearly basis. The launch period for each opportunity is roughly 2.5 weeks long, which either increases or decreases as a function of the maximum launch C_3. The best date to maximize flyby energy is at the beginning of each opportunity, despite launching from Earth later on in the launch period. This implies that minimizing the flight time to Jupiter, which increases the incoming V_∞, yields the highest post-flyby energy. Table 3 and Figure 5 present the range of angles that are covered each year, while still attempting to maximize energy gain. Starting in 2031, the available right ascensions are from 11-32 degrees in the Mean Ecliptic J2000 frame. For each passing year, a gap between 10-20 degrees, cyclic per Jupiter's period, is present, followed by another range of roughly 15-20 degrees of coverage. Declination angles are cyclic with peaks occurring approximately every 6 years at 1.3 degrees which is expected because of Jupiter's orbital inclination of 1.3 degrees and that all cases are able to align the $\vec{V_\infty^+}$ with the planet's velocity vector.

Jupiter-Saturn Gravity Assist Trajectories The JSGA trajectories have the fastest escape speeds from the search. Table 4 contains these opportunities sorted by flyby encounter year, the start and end dates, and their respective characteristics. From Figure 6, its seen that the Saturn arrival dates span from 2039-2042 and 2059. Five different sets of Jupiter encounter dates compose the two continuous sequences. For the 2039-2042 set of solutions, the earliest Jupiter flyby date occurs in January and is available until mid-September 2038 with a decreasing escape speed. Another set of JGAs opens up shortly from February-July 2039 and March-May 2040, and each follows the same trend. Because the second and third JGA reduce the flight time to Saturn (the Saturn arrival is still between 2039-2042), the beginning of each new set increases the post-flyby energy. The Jupiter gravity assist yields V_∞ values in excess of 20.7 and 17.8 km/s for the 2059 and 2039 encounters. However, both these sets are constrained by the minimum flyby altitude and associated bending angle. To prevent flybys through Saturn's D-F rings or below the inner radius of the D ring, a flyby altitude constraint of 80,000 km was used.[13] With this constraint, the bending angles were limited between 45-55 degrees as opposed to the roughly 70 degrees required to maximize the post-flyby velocity. Despite this, Saturn trajectories' energy performance is still superior to the other solutions with C_3 values of 555 km^2/s^2 in 2039 and 698 km^2/s^2 in 2059. The 2059 flyby offers the capability to reach 100 au in a total time from launch of about 19.8 years. Albeit this encounter is at the edge of the search space, the next fastest set of opportunities occur starting 2039 with a heliocentric escape speed of 4.96 au/year. Due to the limited encounter opportunities, the range of right ascensions are much more constrained than the JGA options. As seen in Figure 5, the years 2039 to 2042 have a range of 264-312 degrees and the 2059 opportunity begins at 124 degrees and continues past 140 degrees as the flyby date passes 2060.

Table 3: Opportunities for Jupiter gravity assists occur every 13 months.

Enc. Date Range	Earth Launch*	Escape Velocity** $(au/yr.)$	RA $(deg.)$	Dec. $(deg.)$
5/15/31	1/23/30	4.31	11.13	1.30
9/12/31	2/7/30	3.02	31.52	1.26
5/30/32	2/23/31	4.41	42.37	1.15
10/6/32	3/13/31	3.00	64.61	0.88
6/24/33	3/31/32	4.41	75.62	0.63
10/25/33	4/15/32	3.02	97.18	0.22
7/28/34	5/7/33	4.31	110.57	0.13
11/19/34	5/22/33	3.01	130.70	0.52
9/9/35	6/13/34	4.15	146.55	0.87
12/17/35	6/28/34	3.03	163.87	1.09
10/30/36	7/20/35	3.98	182.91	1.27
1/25/37	8/4/35	3.02	197.88	1.30
12/21/37	8/22/36	3.86	218.14	1.20
3/12/38	9/6/36	3.00	231.80	1.07
2/8/39	9/28/37	3.83	252.02	0.72
4/27/39	10/10/37	3.01	265.06	0.50
3/16/40	10/29/38	3.89	283.95	0.04
6/8/40	11/10/38	3.02	297.89	0.24
4/13/41	11/29/39	4.01	314.82	0.64
7/18/41	12/11/39	3.01	330.82	0.89
5/2/42	12/26/40	4.16	345.01	1.13
8/21/42	1/10/41	3.00	3.65	1.27
5/18/43	1/26/42	4.31	15.50	1.30
9/15/43	2/13/42	3.02	35.87	1.24
6/2/44	3/1/43	4.43	46.75	1.10
10/9/44	3/19/43	3.00	69.03	0.81
6/30/45	4/3/44	4.37	80.58	0.53
10/28/45	4/21/44	3.03	101.58	0.12
8/3/46	5/10/45	4.27	115.51	0.24
11/22/46	5/28/45	3.02	135.01	0.61
9/18/47	6/16/46	4.09	151.89	0.95
12/23/47	7/4/46	3.02	168.59	1.15
11/5/48	7/26/47	3.98	187.53	1.29
1/31/49	8/10/47	3.02	202.45	1.30
12/27/49	8/31/48	3.88	222.56	1.16
3/18/50	9/12/48	3.01	236.24	1.01
2/14/51	10/1/49	3.82	256.53	0.64
5/3/51	10/13/49	3.01	269.54	0.40
3/22/52	11/1/50	3.88	288.49	0.06
6/14/52	11/13/50	3.02	302.42	0.33
4/16/53	12/2/51	4.03	318.95	0.72
7/24/53	12/17/51	3.01	335.42	0.97
5/5/54	12/29/52	4.17	349.26	1.17
8/24/54	1/16/53	3.02	7.86	1.29
5/18/55	2/1/54	4.36	19.32	1.30
9/18/55	2/16/54	3.03	40.28	1.20
6/5/56	3/7/55	4.44	51.17	1.05
10/12/56	3/22/55	3.00	73.57	0.72
7/3/57	4/9/56	4.38	85.09	0.44
10/31/57	4/27/56	3.03	106.13	0.02
8/9/58	5/16/57	4.25	120.51	0.35
11/25/58	6/3/57	3.03	139.50	0.70
9/24/59	6/22/58	4.08	156.76	1.02
12/29/59	7/10/58	3.01	173.47	1.19

*Direct transfer with launch $C_3 \leq 121\ km^2/s^2$
**At the outgoing asymptote

Table 4: Saturn gravity assists occur in 2039-2042 then reoccur in 2059

Enc. Year	Start Date End Date (MM/DD)	Jupiter Gravity Assist Date $(MM/DD/YY)$	Escape Velocity* $(au/yr.)$	RA $(deg.)$	Dec. $(deg.)$
2039	09/30	12/21/37	4.96	264.08	1.38
	12/29	2/1/38	4.56	272.41	1.12
2040	01/01	2/1/38	4.54	272.76	1.11
	12/29	4/24/39	4.00	290.24	0.52
2041	01/01	8/6/38	3.22	299.59	0.17
	12/30	4/24/40	3.34	303.96	0.09
2042	01/02	4/24/40	3.33	304.36	0.07
	03/27	5/18/40	3.00	312.3	0.28
2059	02/14	7/6/57	5.53	123.99	0.07
	12/29	8/24/58	5.02	139.54	0.51

*At the outgoing asymptote

Table 5: Uranus gravity assists are available in 2039-2042 and 2053-2056

Enc. Year	Start Date End Date (MM/DD)	Jupiter Gravity Assist Date $(MM/DD/YY)$	Escape Velocity* $(au/yr.)$	RA $(deg.)$	Dec. $(deg.)$
2039	05/16	9/13/35	4.91	169.23	0.92
	12/30	10/31/35	4.33	179.89	0.91
2040	01/02	11/6/35	4.33	179.94	0.91
	12/30	1/11/36	3.64	196.49	0.84
2041	01/02	1/8/36	3.63	196.72	0.84
	12/28	11/24/36	3.23	205.26	0.78
2042	01/03	11/24/36	3.22	205.59	0.78
	06/08	12/3/36	3.00	212.22	0.74
2053	02/13	11/21/48	4.59	238.68	0.42
	12/31	1/21/50	4.32	246.23	0.26
2054	01/03	2/16/49	3.96	253.12	0.24
	12/29	3/28/50	3.61	262.83	0.07
2055	01/01	3/25/50	3.6	263.04	0.06
	12/30	2/18/51	3.23	270.32	0.07
2056	01/05	2/18/51	3.22	270.62	0.07
	06/06	3/2/51	3.00	276.98	0.13

*At the outgoing asymptote

Jupiter-Uranus Gravity Assist Trajectories JUGA sequences exhibit performance between that of Jupiter-only and Jupiter-Saturn sequences, and have availability from 2039-2042 and 2053-2056. These trajectories have escape speeds ranging between 4.2-4.9 au/year as seen in Table 7. Top performing candidates all have the lowest time-of-flight from Earth to Uranus which results in higher incoming relative velocities (on the order of 18.7 to 20.4 km/s). Similar to the JSGA trajectory set, various Jupiter flyby periods exist to reduce the TOF between the bodies and in return increase the speed. The May 2035, November 2049, and January 2050 encounters of Jupiter result in the fastest associated transfer times. The required flyby bending angles for these trajectories vary between 37 to 41 degrees, but all JUGA opportunities are constrained by the 5000 km flyby altitude. As seen in Table 5, delaying the Uranus encounter by up to 6 months in the 2039 encounter year decreases the escape speed by 0.47 au/year. The September 2053 opportunity can be delayed up to 5 months with a penalty of 0.28 au/year. Both the 2039 and 2053-2054 opportunities have favorable escape characteristics, but the flight time to Uranus is between 5-7 years assuming a direct launch from Earth to the Jupiter gravity assist. The 2053 opportunity is unique due to its escape right ascension. Missions looking to reach the local interstellar medium (ISM) as soon as possible should escape in the direction of the nose of the heliosphere which is currently known to have a right ascension of 245.5 degrees (with respect to the Mean Ecliptic J2000).[1] The 2053 trajectory set escapes at 240.68 degrees at the highest energy, but for a trajectory with the preferred right ascension, the escape speed is 4.37 au/year with a Uranus encounter date on 12/18/2053.

Jupiter-Neptune Trajectories Neptune encounters are limited to five years in the search space beginning in 2038-2040 and 2051-2052. Table 6 contains each set of opportunities and their associated escape speed and direction. The fastest escape trajectory occurs in June 2038 with a speed of 5.11 au/year, and a Jupiter encounter in May 2032. This solution is the fastest performing sequence from the first half of the search space and is nearly matched by JSGAs occurring in 2039 (at 4.96 au/year). However, the interplanetary mission time is much greater (around 2700 days as opposed to 1100 to Saturn). It is worth mentioning that all potential JNGA sequences were not covered due to the input search space constraint of a 3000 day time-of-flight. However, as seen in Figure 1 and

Table 6: Neptune gravity assist occur in 2038-2040 and 2051-2052

Enc. Year	Start Date End Date (MM/DD)	Jupiter Gravity Assist Date $(MM/DD/YY)$	Escape Velocity** $(au/yr.)$	RA $(deg.)$	Dec. $(deg.)$
2038	6/26	5/31/32	5.11	76.14	1.50
	12/26	6/30/32	4.79	81.27	1.46
2039	1/01	6/27/32	4.78	81.48	1.46
	5/25	7/24/32	4.55	85.42	1.42
2040	2/16	6/25/33	4.37	88.14	1.43
	6/15	7/04/33	4.20	91.54	1.39
2051	6/27	6/28/45	5.04	105.45	1.00
	12/30	7/25/45	4.72	110.74	0.91
2052	1/02	7/22/45	4.71	110.85	0.91
	6/30	8/18/45	4.43	115.84	0.82

*At the outgoing asymptote

from Figure 3, the highest V_∞ trajectories usually have the lowest flight times. Therefore, potentially high energy JNGA sequences are covered within the searched TOF limit. All JNGAs reach the minimum flyby altitude constraint, and have subsequent bending angles between 38-52 degrees. Trajectories to Neptune offer an escape direction range from 76-116 degrees which is covered only by Jupiter gravity assists starting in 2033 and every 12^{th} year afterwards.

Fastest Trajectories and Search Space Table 7 summarizes the top performing trajectories with respect to their solar system escape speed. Each trajectory is propagated out to 10 and 20 years past their final encounter epoch to determine the distance traveled. This inevitably makes JUGA and JNGA trajectories appear to cover a larger distance in the fixed propagation time and so the TOF from Earth (also shown in years) is to be considered. Figure 7 shows the various trajectories plotted in the Mean Ecliptic J2000 plane. Every 20^{th} JGA and JUGA and every 10^{th} JSGA are plotted for visual clarity. The search space is able to cover a broad range of outgoing right ascensions, and it's important to note that flyby characteristics can be tweaked to favor a particular escape direction at the expense of the speed.

Table 7: Highest energy gravity assist opportunities by sequence type

Encounter Date	TOF from Earth* $(years)$	JGA Date	Final Body Flyby Alt. (km)	$\mid \vec{V_{h\infty}} \mid$ (au/year)	RA $(deg.)$	Dec. $(deg.)$	10 Years** (au)	20 Years** (au)
JSGA								
02/14/59	2.84	07/06/57	80000	5.53	123.99	0.07	61.14	116.93
9/30/39	3.11	12/21/37	80000	4.96	264.08	1.38	55.14	105.29
JUGA								
05/16/39	4.91	09/13/35	5000	4.91	169.23	0.92	64.62	113.84
09/04/53	5.01	12/27/49	5000	4.61	240.68	0.32	60.79	107.00
JNGA								
06/26/38	7.34	05/31/32	5000	5.11	76.14	1.50	76.17	126.68
06/27/51	7.23	06/28/45	5000	5.05	105.45	1.00	75.47	125.32
JGA								
6/2/44	1.25		40425	4.44	46.68	1.11	47.94	93.38
6/5/56	1.25		40640	4.44	51.17	1.05	47.93	93.35
5/30/32	1.24		40727	4.43	42.31	1.16	47.82	93.15

*Direct transfer with launch $C_3 \leq 121\ km^2/s^2$

**Radial distance from the Sun in the propagation time from the final flyby (excludes interplanetary TOF).

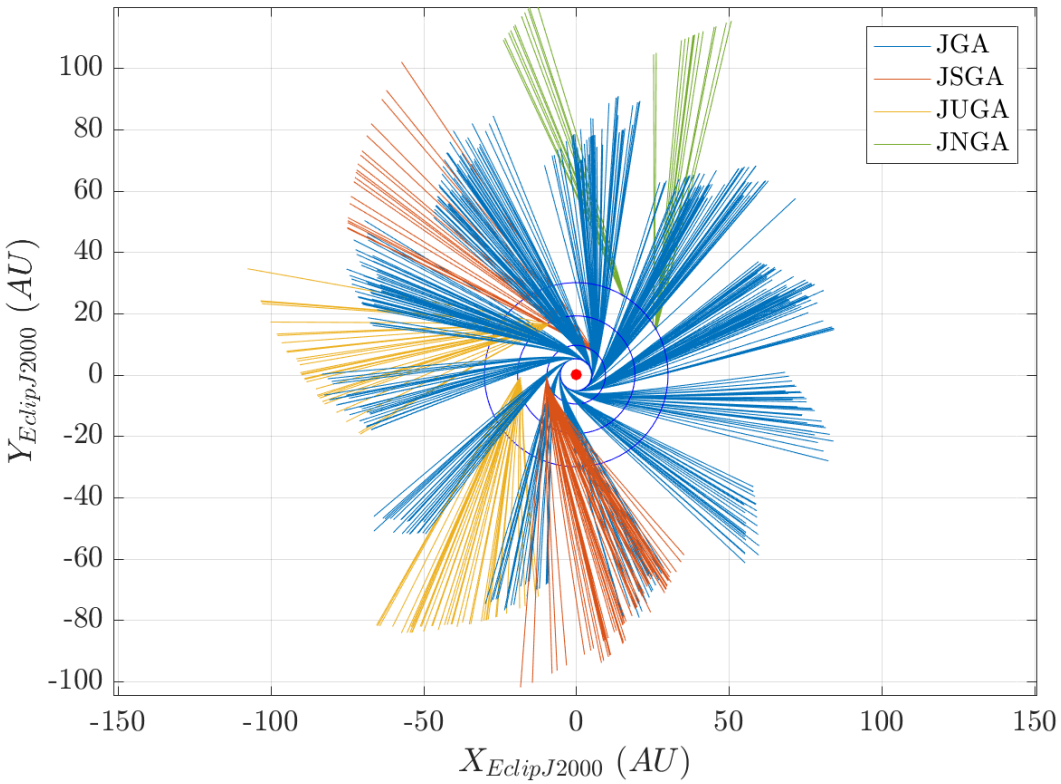

Figure 7: JGA, JSGA, JUGA, and JNGA trajectories plotted in the Mean Ecliptic J2000 frame after 20 years of propagation from the final flyby. The innermost dark blue orbit is the semi-major axis of Jupiter, and each subsequent planet's follows.

KBO SEARCH

The Jet Propulsion Laboratory's Small-Body Database was used to query and filter possible Kuiper Belt Objects with a perihelion radius greater than 35 au and an absolute magnitude less than or equal to 4. The number of KBOs available are 37 making the broad trajectory search manageable. The parameters are identical to Table 2, but now include an additional Kuiper Belt Object flyby. A total of 25 of the 37 KBOs are able to be visited. Table 8 contains the results sorted by the KBO, its semi-major axis, the available gravity assist sequences, and the encounter dates for the sequence with the fastest flight time that encounter the KBO before 2065. Several multi-gravity assist optimized cases are presented in Figure 8, and Jupiter flyby trajectories are presented in Figure 9. The plots in both figures are sorted by the KBO encounter date and are presented in the Mean Ecliptic J2000 plane. The Mission Analysis Low Thrust Optimizer (MALTO) was used to optimize for minimum trip time with ballistic constraint on all legs. The launch energy from Earth was maximized in all cases (121 km^2/s^2 which is the same as in the broad search) to minimize flight time, and orbit leveraging or the inclusion of inner planet flybys were not included in this optimization due to the scope of this topic.

Jupiter-only trajectories have a greater flexibility in reaching a broad range of KBOs and have comparable flight times to multi-gravity assist sequences. For example, the fastest JNGA and JGA to 2005 QU182 differ in flight time by 0.2 years. Seen from Table 8, there is only one KBO that did not have a direct JGA (2010 JO179), but several KBOs exclusively have JGA trajectories. Within

Table 8: Kuiper Belt Trajectory Search Results

Kuiper Belt Object	SMA (au)	Available Sequences	Lowest Flight Time Trajectory				
			Sequence	Jupiter Flyby	Additional Flyby	KBO Arrival	TOF* ($yrs.$)
(2010 JO179)	78.79	JSGA	JSGA	12/27/37	10/11/39	9/4/54	18.03
(2010 KZ39)	45.54	JGA,JSGA	JGA	4/18/41		10/14/52	12.87
(2010 RF43)	49.69	JGA	JGA	5/17/31		3/15/44	14.13
(2014 UZ224)	107.03	JGA,JSGA,JNGA	JNGA	7/6/45	8/24/51	12/11/61	17.69
(2015 KH162)	62.05	JSGA	JSGA	12/27/37	10/14/39	6/11/53	16.81
Varuna	42.72	JGA,JUGA	JGA	9/11/35		7/3/46	12.05
Quaoar	43.69	JGA	JGA	5/7/54		6/19/63	10.45
(2002 AW197)	47.04	JGA,JUGA	JUGA	1/17/50	12/11/53	12/1/60	12.25
(2002 TX300)	43.27	JGA,JSGA,JNGA	JGA	6/26/33		9/26/44	12.49
(2002 UX25)	42.58	JGA,JSGA	JGA	8/2/46		12/18/54	9.60
(2002 TC302)	55.07	JGA,JSGA	JGA	6/26/33		8/12/44	12.36
Sedna	484.44	JGA,JSGA,JNGA	JNGA	6/30/45	7/10/51	11/26/61	17.64
(2004 GV9)	42.12	JGA,JSGA	JSGA	12/24/37	10/5/39	7/13/47	10.88
(2003 OP32)	43.48	JGA,JSGA	JGA	5/17/31		12/16/40	10.90
Makemake	45.43	JGA,JSGA,JUGA	JUGA	1/17/50	12/20/53	12/21/62	14.33
(2005 RN43)	41.76	JGA	JGA	6/7/44		12/28/52	9.83
(2005 RR43)	43.11	JGA,JSGA	JGA	8/2/34		11/1/43	10.49
Varda	46.11	JGA,JSGA	JGA	5/4/54		12/1/63	10.91
(2005 UQ513)	43.33	JGA,JSGA	JGA	6/29/45		10/29/55	11.57
G!kun||'homdima	72.80	JGA,JSGA	JGA	9/17/47		12/13/55	9.48
(2005 QU182)	113.59	JGA,JNGA	JNGA	6/2/32	7/3/38	10/16/46	15.63
(2002 MS4)	42.04	JGA	JGA	5/1/42		6/16/52	11.47
(2014 EZ51)	52.47	JGA,JSGA	JSGA	2/14/39	8/3/40	2/12/50	12.38
(2014 WK509)	50.79	JGA,JSGA	JGA	8/8/46		10/23/56	11.45
(2013 FY27)	58.66	JGA,JSGA	JGA	11/1/36		7/21/54	19.00

*TOF includes a direct launch from Earth to Jupiter

the searched interval, Saturn and Uranus are most effective for outgoing trajectories in the third and fourth quadrant of the ecliptic plane. Most of the Saturn KBO trajectories utilize the 2039-2042 encounter opportunity which results in outgoing right ascension angles between 264-312 degrees. A unique set of flyby dates are seen in the second row and the third row left plot of Figure 8. In the search, 2004 GV9, 2014 EZ51, and 2010 JO179 are all in roughly the same escape right ascension and utilize gravity assists from Jupiter and Saturn within a couple days of each other. While this lineup initially seems promising, each KBO is out of the ecliptic plane at their respective encounter epochs. 2004 GV9 is closest to the ecliptic plane at 5.7 au above it, 2014 EZ51 is 7.7 au below the plane, and 2010 JO179 is 32.5 au above. This lineup also shows the effect of the outgoing declination angle with respect to escape speed. All three flybys use Saturn to increase heliocentric energy, but also to target the specific declination. For an energy maximizing JSGA trajectory with a Saturn encounter on November 11th, 2040, the velocity at the asymptote is 19.92 km/s (4.20 au/year). 2004 GV9, being closest to the ecliptic plane, is seen to have a KBO flyby velocity of 19.88 km/s (4.19 au/year) and 2010 JO179, being very high above the ecliptic with an optimized Saturn flyby B-Plane angle of 44.62 degrees, has an encounter velocity of 17.86 km/s (3.76 au/year). The JSGA to EZ51 arrives at Jupiter earlier with an incoming V_∞ of 11.60 km/s as opposed 11.18 km/s for the GV9 trajectory. This additional speed results in a higher energy SGA and in return a faster encounter velocity of 4.55 au/year despite being 7.7 au below the ecliptic plane.

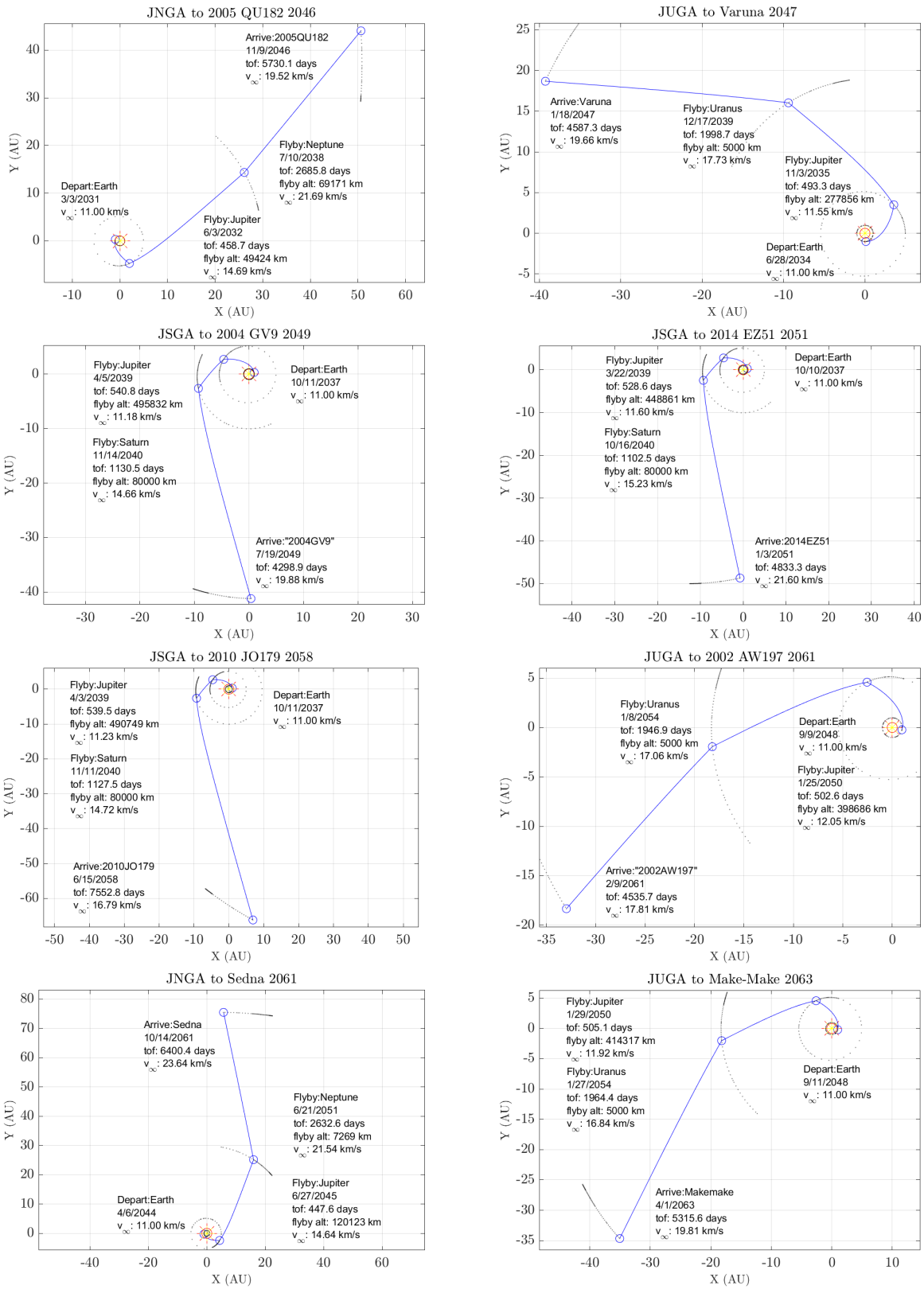

Figure 8: Multiple gravity assists enable relatively fast transfers to large KBOs.

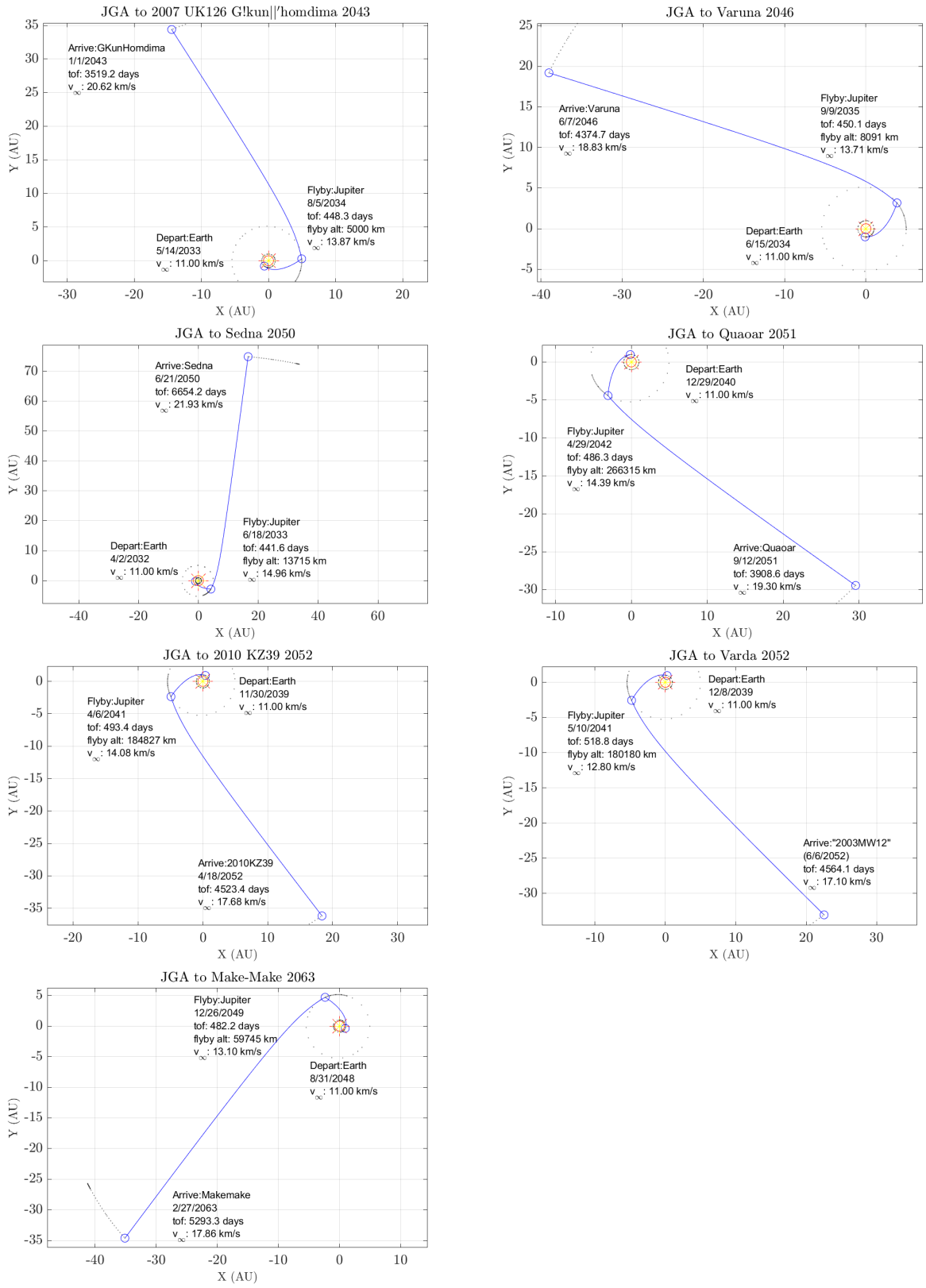

Figure 9: Jupiter flybys enable a variety of escape directions to encounter KBOs.

CONCLUSIONS

A search for ballistic gravity assist combinations to the outer planets is conducted between the years 2030 to 2060. Flyby conditions that maximize the solar system escape speed after final planet are applied to each sequence and the resulting speed and direction are cataloged. All resulting trajectories employ a Jupiter gravity assist with a direct launch from Earth, and escape sequences with the highest speed were those also flew by Saturn. A wide range of right ascensions are available yearly for JGAs at the expense of the escape velocity, but for Kuiper Belt flybys, a direct trajectory from Jupiter is a versatile option with usually lower flight times. Jupiter-Saturn sequences were the fastest in the search space, but are limited in availability with an optimal range of opportunities only occurring every 20 years. Sequences to Uranus and Neptune produced similar escape speeds and perform between JGAs and JSGAs. JSGAs and JUGAs offer a solar system escape in the second and third quadrant of the Mean Ecliptic J2000 frame while JNGAs offers an escape primarily in the first quadrant. Across the solutions, the incoming relative velocity magnitude plays a key role in the maximization of the outgoing energy. For the outer planets excluding Jupiter, the V_∞^- direction is also of importance due to the limited bending capability of these bodies.

ACKNOWLEDGEMENTS

This research was carried out at the Jet Propulsion Laboratory, California Institute of Technology, and is made available for information purposes only. Reference to any specific commercial product, process, or service by trade name, trademark, manufacturer or otherwise, does not constitute or imply its endorsement by the United States Government or the Jet Propulsion Laboratory, California Institute of Technology. Government sponsorship acknowledged.

APPENDIX: B-PLANE DESCRIPTION

The B-Plane (Body Plane) reference frame,[14] shown in Figure 10, is used for characterizing hyperbolic trajectories with respect to a reference body.

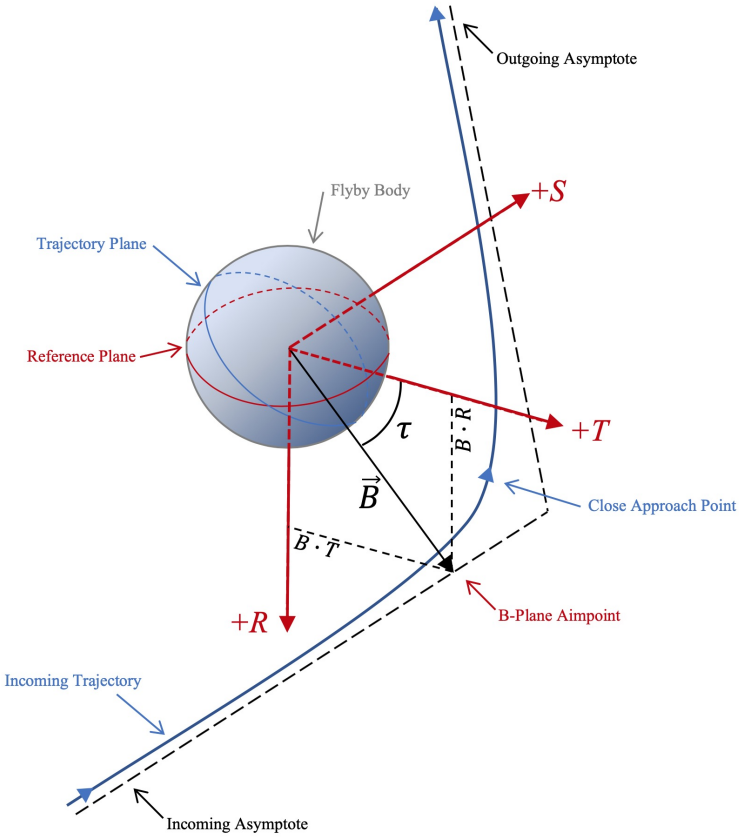

Figure 10: B-Plane Frame and Hyperbolic Trajectory

$$\hat{S} = \frac{\vec{V_\infty^-}}{|\vec{V_\infty^-}|} \qquad \hat{T} = \frac{\hat{S} \times \hat{z}}{|\hat{S} \times \hat{z}|} \qquad \hat{R} = \hat{S} \times \hat{T} \tag{17}$$

The unit vectors: $\hat{x}$=$[1,0,0]^T$, $\hat{y}$=$[0,1,0]^T$, $\hat{z}$=$[0,0,1]^T$ are the axes of the Mean Ecliptic J2000 frame used throughout this paper. The B-Plane angle (τ) is defined as the angle the trajectory's B-Plane Aimpoint vector ($\vec{B}$) makes with respect to the $+\hat{T}$ axis measured towards the $+\hat{R}$ direction (clockwise). Note that the close approach point and the point where the trajectory crosses the B-Plane, defined by the T and R axis, are not the same. These will only coincide if the gravity of the body is removed (no trajectory bending). The following frame transformation is applied to the $\vec{V_p}$ to represent its components in the B-Plane's STR Frame:

$$\begin{pmatrix} V_{p_s} \\ V_{p_t} \\ V_{p_r} \end{pmatrix} = \begin{bmatrix} \hat{S}\cdot\hat{x} & \hat{S}\cdot\hat{y} & \hat{S}\cdot\hat{z} \\ \hat{T}\cdot\hat{x} & \hat{T}\cdot\hat{y} & \hat{T}\cdot\hat{z} \\ \hat{R}\cdot\hat{x} & \hat{R}\cdot\hat{y} & \hat{R}\cdot\hat{z} \end{bmatrix} \begin{pmatrix} V_{p_x} \\ V_{p_y} \\ V_{p_z} \end{pmatrix} \tag{19}$$

REFERENCES

[1] N. Arora, N. Strange, and L. Alkalai, "Trajectories for a near term mission to the interstellar medium," *AAS/AIAA Astrodynamics Specialist Conference 2015*, Vol. 156, Vail, Colorado, 2015, pp. 3037–3055.

[2] C. E. Garner, W. Layman, S. A. Gavit, and T. Knowles, "A Solar Sail Design for a Mission to the Near-Interstellar Medium," *Space Technology and Applications International Forum*, Albuquerque, New Mexico, American Institute of Physics, 2000, pp. 947–961.

[3] J. A. Atchison, M. T. Ozimek, C. J. Scott, and F. E. Siddique, "Robust High-Fidelity Gravity-Assist Trajectory Generation Using Forward/Backward Multiple Shooting," *25th AAS/AIAA Space Flight Mechanics Meeting*, No. January, Williamsburg, Virginia, 2015, pp. 2359–2376.

[4] A. E. Lynam, "Broad Search for Direct Trajectories from Earth to Double-satellite-aided Capture at Jupiter with Deep Space Maneuvers," *AAS/AIAA Spaceflight Mechanics Meeting*, Napa Valley, California, American Institute of Aeronautics and Astronautics, 2016.

[5] C. Spreen, M. Mueterthies, K. Kloster, and J. Longuski, "Preliminary analysis of ballistic trajectories to Uranus using gravity-assists from Venus, Earth, Mars, Jupiter, and Saturn," *Advances in the Astronautical Sciences*, Vol. 142, 2012, pp. 3411–3428.

[6] K. Hughes, J. Moore, and J. Longuski, "Preliminary analysis of ballistic trajectories to neptune via gravity assists from venus, earth, mars, jupiter, saturn, and uranus," *Advances in the Astronautical Sciences*, Vol. 150, 2014, pp. 1535–1554.

[7] D. Sanchez, A. Sukhanov, and A. Prado, "Optimal trajectories to Kuiper Belt Objects," *Revista Mexicana de Astronomía y Astrofísica*, Vol. 55, 05 2019, pp. 39–54, 10.22201/ia.01851101p.2019.55.01.06.

[8] A. M. Zangari, T. J. Finley, S. Alan Stern, and M. B. Tapley, "Return to the Kuiper Belt: Launch Opportunities from 2025 to 2040," *Journal of Spacecraft and Rockets*, Vol. 56, No. 3, 2019, pp. 919–930, 10.2514/1.A34329.

[9] R. Mcgranaghan, B. Sagan, G. Dove, A. Tullos, J. Lyne, and J. Emery, "A Survey of Mission Opportunities to Trans-Neptunian Objects," *Journal of the British Interplanetary Society*, Vol. 142, 09 2011, pp. 296–303.

[10] Y. Guo and R. W. Farquhar, "New Horizons Mission Design," *Space Science Review*, Vol. 140, 2008, pp. 49–74.

[11] D. Landau, T. Lam, and N. Strange, "Broad search and optimization of solar electric propulsion trajectories to Uranus and Neptune," *Advances in the Astronautical Sciences*, Vol. 135, No. 3, 2009, pp. 2093–2112.

[12] T. Lam, D. Landau, and N. Strange, "Broad search for solar electric propulsion trajectories to Saturn with gravity assists," *Advances in the Astronautical Sciences*, Vol. 135, Pittsburgh, Pennsylvania, 2009, pp. 905–918.

[13] M. S. Tiscareno, "Planetary Rings," *Planetary Ring Systems* (T. D. Oswalt, ed.), ch. Planetary, pp. 61–63, Springer, 3 ed., 2012.

[14] M. Macdonald and C. R. McInnes, "Spacecraft Planetary Capture Using Gravity-Assist Maneuvers," *Guidance, Control, and Dynamics*, Vol. 28, No. 2, 2005, pp. 365–368.